Detonation Propulsion Experiments and Theory

Lloyd H. Back,* Warren L. Dowler,† and Giulio Varsi‡
Jet Propulsion Laboratory, California Institute of Technology, Pasadena, California

New experimental data are presented for single detonation of explosives in nozzles for propulsion in a simulated Jupiter atmosphere, along with additional data for other ambient gases (nitrogen, carbon dioxide, and helium). These data were obtained with various types of nozzles: long cone, short cone, straight, and firing plug. With the long-cone nozzle, there was a progressive increase in specific impulse with ambient pressure for the higher molecular weight gases, carbon dioxide and nitrogen, whereas for the lower molecular weight gases, helium and the simulated Jupiter atmosphere, the specific impulse decreased with increasing ambient pressure. With the short-plug nozzle, there was a slight reduction in specific impulse with increasing ambient pressure, and the results were virtually independent of the molecular weight of the ambient gas. These new data, along with data previously obtained with other ambient gases and nozzle types, were analyzed using first principles, approximate predictions from blast wave theory, and numerical, two-dimensional calculations to acquire a basic understanding of the experimental trends and to predict specific impulses. Rarefaction and oscillatory wave phenomena, as indicated by pressure transducer measurements along the nozzle wall and by predictions, significantly influence the specific impulse. Nozzle design considerations for a flight system are discussed, including estimated projections for pulse firing and relative vehicle speed.

Nomenclature

A = nozzle cross-sectional area
C = speed of sound
e_α = specific energy released in explosion, E_α/m_{ex}
E_α = energy released in explosion
F = function, Eq. (11)
$f_1 f_2$ = functions of γ, Eq. (4)
G,H = integrals, Eq. (5)
g_c = conversion constant
I = specific impulse
L = axial length of nozzle
m = mass of gas
m_a = mass of ambient gas in nozzle
m_{ex} = mass of explosive material
M_I = inert hardware mass
M_p = propellant mass
P = static pressure
P_a = ambient pressure
P_c = internal combustion chamber pressure
P_e = pressure at nozzle exit
P_0 = plateau pressure
P_R = pressure just behind shock wave
r = radial distance from apex of nozzle cone
r_e = radial length of conical nozzle
R = radial position of shock wave
R_ℓ = characteristic length, Eq. (6)
t = time
T_a = ambient temperature
V = nozzle volume
α = function of γ, Table 2
γ = specific heat ratio
ζ = function of θ, Eq. (8)
η = function of θ, Eq. (3)
θ = conical half-angle
ι = normalized specific impulse
λ = divergence factor, Eq. (13)
ξ = nondimensional length, Eq. (9)
ρ = density
σ = ratio of mass of ambient gas in nozzle to mass of explosive, m_a/m_{ex}
τ_e = nondimensional time when shock wave reaches nozzle exit, $t_e C_a/R_\ell$
ω = solid angle

Subscripts

a = ambient condition
R = condition just behind shock wave

Received April 5, 1982; presented as Paper 82-1115 at the AIAA/ASME/SAE 18th Joint Propulsion Conference, Cleveland, Ohio, June 21-23, 1982; revision received Jan. 12, 1983.

*Transport and Reactive Processes Research Group Supervisor.
†Member Technical Staff.
‡Manager, Thermochemical Research and Systems Section.

Introduction

BECAUSE of the scientific interest in exploring the dense or high-pressure atmospheres of the solar system planets Jupiter, Neptune, Saturn, Uranus, and Venus, the Jet Propulsion Laboratory (JPL) has been conducting a technology investigation of detonation propulsion.[1-7] This propulsion technique is of interest when attitude control, entry maneuvers, or escape propulsion is required to accomplish a mission within the atmospheres of these planets at pressures greater than 50 atm.

The major advantage of detonation propulsion over conventional rocket motors, which use deflagrating propellants and a DeLaval nozzle gas expansion, is the potential for increased performance. The propellant performance (specific impulse, I) of conventional rockets is dependent on the ratio of the internal combustion chamber pressure to the nozzle exit static pressure; this pressure ratio is determined by the nozzle expansion area ratio, A_e/A_{throat}. I is optimum when P_c/P_e equals P_c/P_a, and this pressure ratio must be at least about 2 to obtain sonic velocity at the throat. For current motor designs fired within the Earth's atmosphere, the nozzle expansion area ratio is between 5 and 100; for space motors, the nozzle expansion area ratio is between 30 and 1000. The second affected performance parameter is the propulsion mass fraction, $M_p/(M_p+M_I)$, for which the mass, M_I, of the rocket inert hardware is significantly influenced by the difference between internal and external pressures. For conventional main propulsion space

rockets, a propulsion mass fraction between 0.8 and 0.95 can be achieved. At the low external pressures for Earth or space vacuum, the optimum values for chamber pressures are between 10 and 50 atm because the external pressure has little effect; however, as the external ambient atmospheric pressure increases above 50 atm, high performance cannot be achieved with conventional designs. Five design problems become evident.

1) Solid propellant burning rates would be high because combustion must take place at high pressure. Thus, the propellant web thickness would become large in order to achieve long burning times needed for moderate thrust levels.

2) For both solid and liquid propellant engines, the heat transfer to injector, chamber, and nozzle walls becomes severe because the heat-transfer coefficient is dependent on the chamber pressure.

3) With large external-to-internal pressure differences, the pressure vessel walls would become extremely massive.

4) The gas expansion process would optimize at low values of nozzle expansion ratio to give low propellant specific impulses.

5) The prediction of accurate motor performance would be nearly impossible if the ambient pressure varies or is not known; for many early missions in dense planetary atmospheres, this would probably be the case, and heavy, low-performance conservative designs would be used.

The detonation propulsion concept has the potential of increasing the performance to acceptable levels by essentially eliminating the first-order influence of high ambient atmospheric pressures on jet propulsion inert mass design parameters. The results of our current work relate the specific impulse to the complex effects of expelling ambient gases from the nozzle.

The feasibility of a pulse detonating propellant approach was demonstrated in 1973 by Varsi et al.[1] Both experimental results and theoretical analysis have indicated that a small quantity of explosive detonated within a nozzle expansion cone and high molecular weight ambient gases produced high propellant specific impulses. In fact, the propellant specific impulse is increased at higher ambient pressure due to expulsion of the mass of ambient gas in the nozzle.[2] However, low molecular weight gases are of particular interest: the nominal model for the Jupiter atmosphere estimates 86.6% hydrogen and 13.2% helium.[8] The nominal model for Saturn estimates 88.6% hydrogen and 11.2% helium.[9] Predictions of specific impulse and experimental work indicated a decrease in specific impulse for low molecular weight ambient gases when longer expansion cones were used.[4]

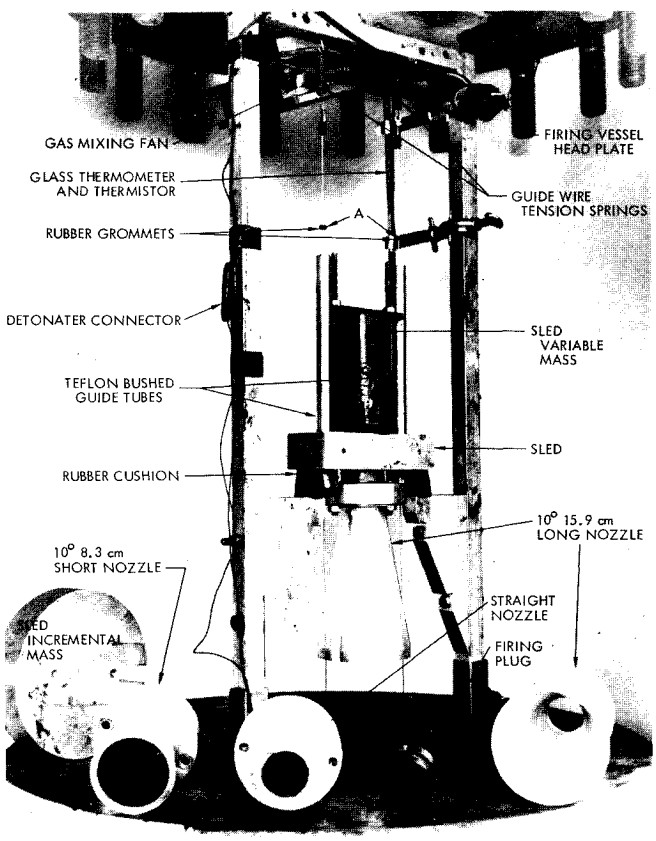

Fig. 1 Experimental sled device and nozzles.

Low molecular weight ambient gas experiments were conducted using helium, which has a molecular weight of 4 (Ref. 4). In order to decrease the molecular weight so as to maximize the molecular weight effect, test firings in a hydrogen atmosphere were considered; however, because of the scientific interest in future Jupiter and Saturn missions a simulated Jupiter atmosphere composed of commercial-quality hydrogen and helium was considered more appropriate and hence used.

This paper reports these new experimental data for the simulated Jupiter atmosphere, and additional data for other ambient gases (nitrogen, carbon dioxide, and helium) for various types of nozzles. These data for single detonations, along with previous data obtained with the other ambient gases and nozzle types, are then analyzed using first principles, approximate predictions from blast wave theory, and numerical (two-dimensional) calculations to acquire a basic understanding of the experimental trends and to predict the specific impulses.

Experiments

Apparatus

The experimental apparatus used for this series of test firings was essentially the same as that used in Ref. 4, except for modifications of the apparatus to permit the addition and mixing of hydrogen and helium in the firing vessel. Figure 1 shows the opened firing vessel, which could be pressurized from vacuum to 70 atm, and the nozzle sled, along with an end view of the nozzles tested. The nozzle dimensions are shown in Fig. 2. This figure also includes a view of the 1.5 g duPont de Nemours Deta sheet C and the Space Ordnance Systems P/N 06401 microdetonator, which was placed into the firing-plug cavity. The specific energy released by the Deta sheet C is 1080 cal/g. This material was used in all of the later test firings. Deta sheet A, with a specific energy release of 1180 cal/g, was used for the early test firings prior to a change in formulation by duPont in 1974.

The sled apparatus was modified from an earlier design[4] to improve data reproducibility by making height markers out of 0.5-cm diam rubber grommets (A in Fig. 1); two were used each time. Also, all parts of the sled near the nozzle that could interfere with or be acted on by the blast wave were placed on top of the sled (see Fig. 1 of Ref. 4 for comparison). The ambient gas temperature, which was near 20°C, was measured by a thermistor that was calibrated by a glass thermometer.

The diagram of Fig. 3 shows schematically the gas-filling system. The important aspects of this apparatus are: 1) the remote control of the firing apparatus; 2) the ability to evacuate the firing vessel so that all of the air (oxygen) can be removed to prevent deflagration of hydrogen in the firing vessel with residual air which would be ignited by the hot combustion products of the explosive charge; 3) the utilization of a small "pancake" fan to mix the helium with the hydrogen and to aid in rapid heat transfer from the ambient gases to the vessel walls due either to the adiabatic compression of the gases when the tank is being filled or the explosive products after the test firing; 4) the venting and exchange of the vessel atmosphere with air after the test firing by first evacuating and filling with helium; 5) low- and high-

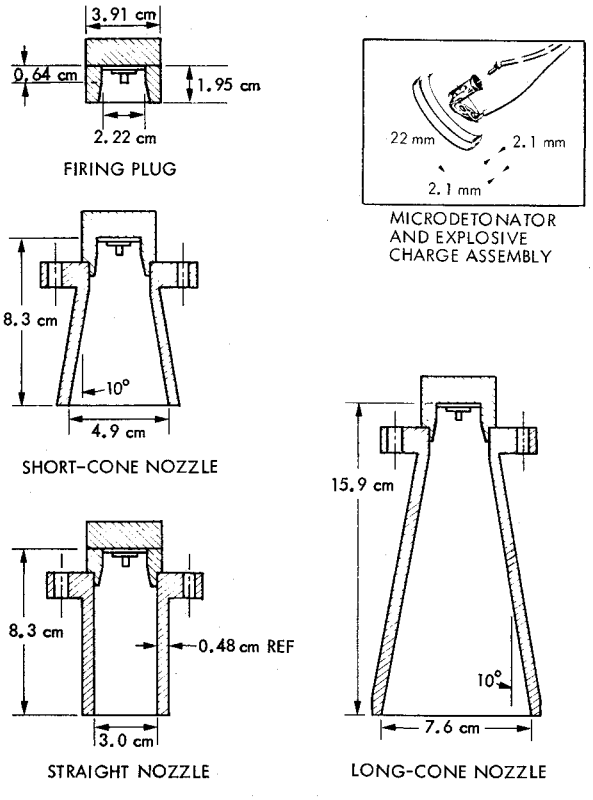

Fig. 2 Nozzles tested and explosive charge with microdetonator.

pressure precision-calibrated gages that were used to obtain the desired composition of the simulated Jupiter atmosphere of hydrogen and helium by filling the vessel using the pressure ratio of the two gases; and 6) a subsystem to obtain a gas sample for mass spectrometer composition analysis.

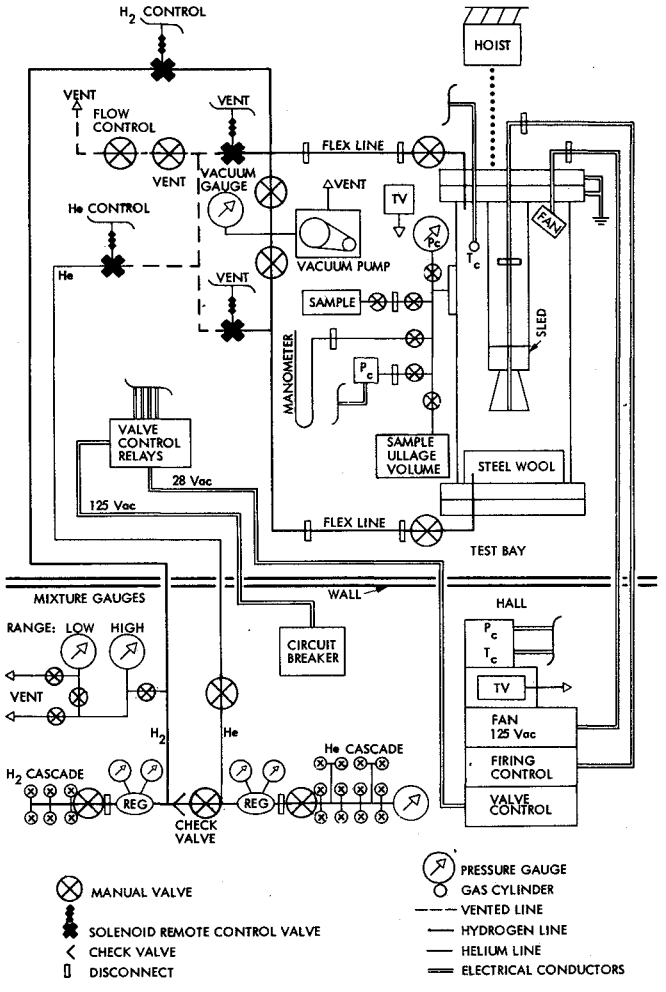

Fig. 3 Simulated Jupiter atmosphere test apparatus schematic.

Procedure

The equipment for obtaining the simulated Jupiter atmospheric gas mixture and a gas sample for analysis is illustrated schematically in Fig. 3. An evacuated gas sample bottle was connected to the sample manifold. The weighed test nozzle with explosive charge was mounted on the sled, and the detonator wires were connected. After the assembly was lowered into the chamber, the head was sealed and bolted to the chamber. The firing vessel and sample ullage volume were evacuated; the sample ullage volume valve, manometer valve, and sample bottle connection valve were then closed. Residual air was removed from the firing vessel by filling it with helium and evacuating again. After the second helium filling, the firing vessel was vented to a pressure level that produced the proper ratio of hydrogen to helium after the hydrogen was added. For test firings up to 29 bars pressure, the vessel was pressurized to 3.67 bars with helium, and then pressurized to 29.0 bars using hydrogen. For the 69-bar firings, the pressures were 8.62 bars for helium and 69 bars for helium plus hydrogen. This low- and high-pressure procedure was used to eliminate wasting significant amounts of gases for the low-pressure firing tests. The fan was turned on during the purge procedure to mix the tank contents and approach thermal equilibrium. The mixing took about 5 min and was considered complete when the temperature indicated by the thermistor was constant within 1°C. For tests below 29 bars, the firing vessel was vented to test pressure and held again for about 5 min. A gas sample was taken by opening the evacuated ullage volume valve to clear the lines of unmixed gases, and then the two sample bottle valves were opened filling the sample bottle. These two valves were then closed. After the firing the sample bottle was removed.

Because of the use of commercial grade gases, the cascade gas quality was determined using mass spectrometry for one sample of hydrogen and two of helium. Hydrogen was essentially pure and contained 0.06% nitrogen as an impurity. The commercial helium was not pure, and the analyses indicate some variability which is unknown because several cascades which were not sampled were consumed for the venting procedure. The average helium composition from two gas samples was 98.6% helium, 0.9% nitrogen, 0.2% oxygen, and 0.3% argon.

Specific Impulse Data Trends

Table 1 includes the new specific impulse data for the simulated Jupiter atmosphere obtained with four types of nozzles—long cone, short cone, straight, and firing plug. New data obtained with the short-plug and straight nozzle for nitrogen, carbon dioxide, and helium ambient gases, and previous data obtained with the other ambient gases and nozzle types indicated are also included. To verify the repeatability of the experimental firings with the apparatus illustrated in Fig. 3, a series of replicated firing tests using helium at 28.6 bars was made. (D1, D2, D4, and D5 tabulated in Table 1a). The range of this I is 6 s out of 181, or about 3%.

To observe the experimental trends, the variation of specific impulse with ambient pressure is shown in Fig. 4 for the long-cone and firing-plug nozzles and for the various ambient gases. With the long-cone nozzle there was a progressive increase in specific impulse with ambient pressure for the higher molecular weight gases, carbon dioxide and nitrogen, whereas for the lower molecular weight gases,

helium and the simulated Jupiter atmosphere, the specific impulse decreased with increasing ambient pressure.

However, with the firing-plug nozzle there was a slight reduction in specific impulse with increasing ambient pressure, and the results were virtually independent of the molecular weight of the ambient gas, as shown in Fig. 4. Thus, at low and high ambient pressures, a relatively small volume nozzle compared to a larger volume nozzle would significantly decrease the specific impulse with carbon dioxide and nitrogen ambient gases and would slightly decrease the specific impulse for helium, but a short nozzle would increase the specific impulse at higher ambient pressures for the simulated Jupiter atmosphere.

Theoretical Considerations

In order to acquire a basic understanding of these seemingly complex trends, resort was made to a simplified analysis from first principles,[2] a modification of an approximate prediction from blast wave theory,[3] and a numerical, two-dimensional calculation scheme.[6] In this regard, an important parameter in detonation propulsion is the ratio of the mass of ambient

Table 1a Experimental data for long cone-nozzle

	Nozzle						Ambient gas				
Run No.	Type	Half-angle degrees	Length, cm	Volume, V, cm^3	e_α, cal/g	σ, m_a/m_{ex}	Type	Pressure, bars	Temp., K	Density, g/cm^3	Specific impulse, Is[a]
D8	Cone	10	15.9	316	1080	2.49×10^{-2}	Jupiter[b]	1.30	290	1.24×10^{-4}	230
D7	Cone	10	15.9	316	1080	1.56×10^{-1}	Jupiter	8.28	295	7.80×10^{-4}	192
D6	Cone	10	15.9	316	1080	5.52×10^{-1}	Jupiter	29.0	294	2.74×10^{-3}	157
D24	Cone	10	15.9	316	1080	1.28	Jupiter	69.0	302	6.35×10^{-3}	122
D1	Cone	10	15.9	316	1080	9.71×10^{-1}	He	28.6	293	4.82×10^{-3}	186
D2	Cone	10	15.9	316	1080	9.65×10^{-1}	He	28.6	293	4.82×10^{-3}	180
D4	Cone	10	15.9	316	1080	9.65×10^{-1}	He	28.6	293	4.82×10^{-3}	181
D5	Cone	10	15.9	316	1080	9.65×10^{-1}	He	28.6	293	4.82×10^{-3}	181
K4	Cone	10	15.9	320	1180	3.5×10^{-2}	He	0.967	298	1.68×10^{-4}	223
K7	Cone	10	15.9	320	1180	0.300	He	8.5	298	1.41×10^{-3}	211
K6	Cone	10	15.9	320	1180	1.80	He	51.0	298	8.45×10^{-3}	192
K.4	Cone	10	15.9	320	1180	2.11	He	59.5	298	9.86×10^{-3}	182
1.1	Cone	10	15.9	320	1180	9.40×10^{-4}	N_2	4×10^{-3}	298	4.64×10^{-6}	236
C1	Cone	10	15.9	320	1180	2.44×10^{-1}	Air	0.967	298	1.20×10^{-3}	236
1.2	Cone	10	15.9	320	1180	1.95	N_2	8.28	298	9.61×10^{-3}	270
1.3	Cone	10	15.9	320	1180	16.2	N_2	69	298	8.06×10^{-2}	290
C1.5	Cone	10	15.9	320	1180	0.370	CO_2	0.967	308	1.75×10^{-3}	255
C1.4	Cone	10	15.9	320	1180	9.50	CO_2	25.3	308	4.55×10^{-2}	307
C1.3	Cone	10	15.9	320	1180	$2.08\times10^{+1}$	CO_2	47.3	308	9.95×10^{-2}	338
C1.2	Cone	10	15.9	320	1180	$4.12\times10^{+1}$	CO_2	69.7	308	2.02×10^{-1}	378
C1.1	Cone	10	15.9	320	1180	$1.20\times10^{+2}$	CO_2	84.5	308	5.73×10^{-1}	579

Table 1b Experimental data for short-cone nozzles

	Nozzle						Ambient gas				
Run no.	Type	Half-angle degrees	Length, cm	Volume, V, cm^3	e_α, cal/g	σ, m_a/m_{ex}	Type	Pressure bars	Temp., K	Density, g/cm^3	Specific impulse, Is[a]
D15	Cone	10	8.3	83	1080	5.98×10^{-4}	Jupiter[b]	1.26	293	1.19×10^{-4}	216
D16	Cone	10	8.3	83	1080	4.29×10^{-2}	Jupiter	8.63	294	8.16×10^{-4}	207
D17	Cone	10	8.3	83	1080	1.45×10^{-1}	Jupiter	28.8	292	2.74×10^{-3}	186
D19	Cone	10	8.3	83	1080	1.42×10^{-1}	Jupiter	28.8	295	2.71×10^{-3}	184
D25	Cone	10	8.3	83	1080	3.44×10^{-1}	Jupiter	69.0	293	6.54×10^{-3}	155
1.12	Cone	10	4.5	26	1180	1.50×10^{-4}	N_2	8×10^{-3}	298	9.04×10^{-6}	222
1.13	Cone	10	4.5	26	1180	1.90×10^{-2}	N_2	0.967	298	1.13×10^{-3}	237
1.14	Cone	10	4.5	26	1180	1.57×10^{-1}	N_2	8.28	298	9.36×10^{-3}	260
1.15	Cone	10	4.5	26	1180	1.31	N_2	69.0	298	7.80×10^{-2}	282
1.8	Cone	10	8.3	80	1180	2.40×10^{-4}	N_2	4×10^{-3}	298	4.64×10^{-6}	232
1.9	Cone	10	8.3	80	1180	5.90×10^{-2}	N_2	0.967	298	1.16×10^{-3}	239
1.10	Cone	10	8.3	80	1180	4.90×10^{-1}	N_2	8.28	298	9.61×10^{-3}	254
1.11	Cone	10	8.3	80	1180	4.1	N_2	69.0	298	8.06×10^{-2}	267
1.4	Cone	10	12.1	174	1180	5.1×10^{-4}	N_2	4×10^{-3}	298	4.52×10^{-6}	249
1.5	Cone	10	12.1	174	1180	1.28×10^{-1}	N_2	0.967	298	1.13×10^{-3}	236
1.6	Cone	10	12.1	174	1180	1.06	N_2	8.28	298	9.36×10^{-3}	250
1.7	Cone	10	12.1	174	1180	8.87	N_2	69.0	298	7.80×10^{-2}	279

[a] Units are lbf-s/lbm. For SI units multiply the value by 9.806 to obtain N-s/kg. [b] Simulated Jupiter atmosphere of commercial gases; nominal concentration was 87.5% H_2 and 12.5% He.

Table 1c Experimental data for straight nozzles

Run No.	Nozzle Type	Half-angle degrees	Length, cm	Volume, V, cm^3	e_α, cal/g	σ, m_a/m_{ex}	Ambient gas Type	Pressure bars	Temp., K	Density, g/cm^3	Specific impulse, Is[a]
D20	Straight	0	8.3	55	1080	4.20×10^{-3}	Jupiter[b]	1.29	292	1.23×10^{-4}	204
D21	Straight	0	8.3	55	1080	2.77×10^{-2}	Jupiter	8.63	296	8.10×10^{-4}	202
D18	Straight	0	8.3	55	1080	9.42×10^{-2}	Jupiter	28.8	290	2.76×10^{-3}	185
D23	Straight	0	8.3	55	1080	2.19×10^{-1}	Jupiter	69.0	300	6.39×10^{-3}	166
K38	Straight	0	8.3	55	1080	4.02×10^{-1}	He	69.0	298	1.14×10^{-2}	173
K37	Straight	0	8.3	55	1080	2.76	N_2	69.0	298	8.01×10^{-2}	244
2.3	Straight	0	21.7	149	1180	4.00×10^{-4}	N_2	6.7×10^{-3}	298	7.77×10^{-6}	231
2.1	Straight	0	21.7	149	1180	6.00×10^{-2}	N_2	0.967	298	1.12×10^{-3}	214
2.2	Straight	0	21.7	149	1180	4.14	N_2	69.0	298	8.01×10^{-2}	273

Table 1d Experimental data for firing-plug nozzles

Run no.	Nozzle Type	Half-angle degrees	Length, cm	Volume, V, cm^3	e_α, cal/g	σ, m_a/m_{ex}	Ambient gas Type	Pressure bars	Temp., K	Density, g/cm^3	Specific impulse, Is[a]
D14	Plug	0	1.95	8.9	1080	6.19×10^{-4}	Jupiter[b]	1.26	291	1.20×10^{-4}	191
D13	Plug	0	1.95	8.9	1080	6.43×10^{-4}	Jupiter	1.32	293	1.25×10^{-4}	193
D12	Plug	0	1.95	8.9	1080	4.23×10^{-3}	Jupiter	8.63	292	8.21×10^{-4}	191
D10	Plug	0	1.95	8.9	1080	1.38×10^{-2}	Jupiter	28.8	296	2.68×10^{-3}	190
D22B	Plug	0	1.95	8.9	1080	3.32×10^{-2}	Jupiter	69.0	298	6.43×10^{-3}	178
Plg5	Plug	0	1.95	8.9	1080	9.40×10^{-4}	He	0.967	298	1.60×10^{-3}	197
Plg6	Plug	0	1.95	8.9	1080	8.20×10^{-3}	He	8.70	298	1.44×10^{-3}	198
Plg1	Plug	0	1.95	8.9	1080	6.50×10^{-2}	He	69.0	298	1.14×10^{-2}	183
Plg21	Plug	0	1.95	8.9	1080	6.52×10^{-3}	N_2	0.967	298	1.12×10^{-3}	202
Plg7	Plug	0	1.95	8.9	1080	5.67×10^{-2}	N_2	8.7	298	1.01×10^{-2}	194
Plg4	Plug	0	1.95	8.9	1080	4.50×10^{-1}	N_2	69.0	298	8.01×10^{-2}	182
Plg8	Plug	0	1.95	8.9	1080	3.04×10^{-1}	CO_2	28.8	298	5.25×10^{-2}	184

[a] Units are lbf-s/lbm. For SI units multiply the value by 9.806 to obtain N-s/kg. [b] Simulated Jupiter atmosphere of commercial gases; nominal concentration was 87.5% H_2 and 12.5% He.

gas, m_a, contained in the nozzle to the mass of gas generated from the explosive materials, m_{ex}, for an ideal explosion:

$$\sigma = m_a/m_{ex} = \rho_a V/m_{ex} \tag{1}$$

where V is the nozzle volume. In Table 1, the volumes of the nozzles are given along with the values of σ for the various test conditions.

For the long-cone nozzle with carbon dioxide and nitrogen as ambient gases, values of σ were considerably greater than unity at the higher ambient pressures (Table 1a). In this case the experimental trend of increasing specific impulse with ambient pressure (Fig. 4) is consistent with the approximate prediction[3] also shown in Fig. 4, based on the application of blast wave theory to the detonation of an explosive in a conical nozzle for the situation where σ is much greater than unity, i.e., 10. For the lower molecular weight ambient gases, values of σ were much smaller, being equal to 2.11 for helium and 1.28 for the simulated Jupiter atmosphere at the highest ambient pressure of 59.5 and 69 bars, for the long-cone nozzle. At lower ambient pressures, values of σ are proportionately smaller, as is also the case for the shorter length nozzles. Consequently, the application of blast wave theory to these conditions is tenuous and the estimated specific impulses would be considerably below the data, although the trend of decreasing specific impulse with decreasing molecular weight of the ambient gas was evident.

Because of the rather simple closed-form expression for the specific impulse obtained from blast wave theory, there is merit in extending the analysis to include helium and the simulated Jupiter atmosphere. Rewriting Eq. 17a from Ref. 3 by expressing the radial length of the nozzle, r_e in terms of the conical volume (which was easily measured for the test nozzles) gives the specific impulse as:

$$I = \left[\frac{16}{15}(3\pi)^{1/2}\right]\eta f_1\left(2\frac{e_\alpha}{g_c}\sigma\right)^{1/2}\left[1+\frac{15}{32(\pi)^{1/2}}f_2 H\left(\frac{r_e}{R_\ell}\right)^{1/2}\right] \tag{2}$$

where the function η depends upon the conical half-angle θ

$$\eta = \frac{\sin\theta}{\cos^{1/2}\theta(1-\cos\theta)^{1/2}} \tag{3}$$

the functions f_1 and f_2 depend upon γ

$$f_1 = \frac{G}{(\gamma+1)\alpha^{1/2}} \qquad f_2 = \frac{(\gamma+1)\alpha^{1/2}}{G\gamma^{1/2}} \tag{4}$$

the integrals G and H are given by

$$G = \int_0^1 \frac{p}{P_R}\frac{r}{R}\,\mathrm{d}(r/R) \qquad H = \int_{\tau_e}^{\infty}\left(\frac{p_0}{p_a}-1\right)\mathrm{d}\tau \tag{5}$$

and e_α is the energy released in the explosion per mass of explosive.

Appropriate values for the functions f_1, f_2, α, and G obtained from Refs. 10-12 are given in Table 2 for an ideal

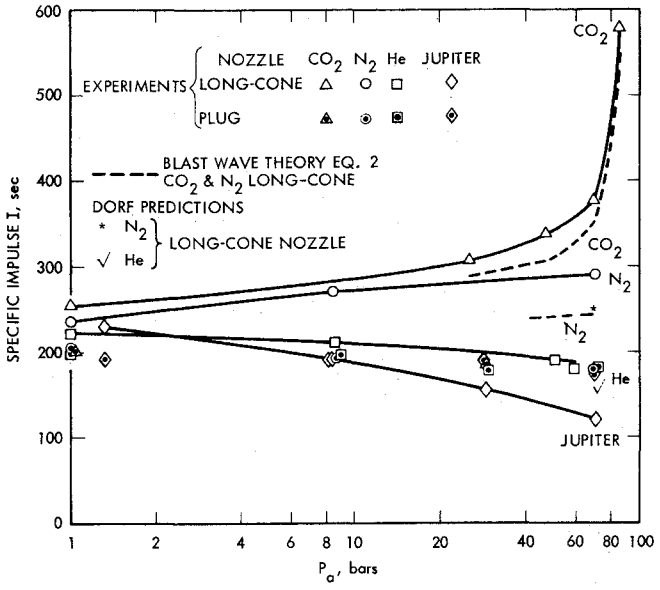

Fig. 4 Variation of specific impulse with ambient pressure for various ambient gases with the long-cone and firing-plug nozzles.

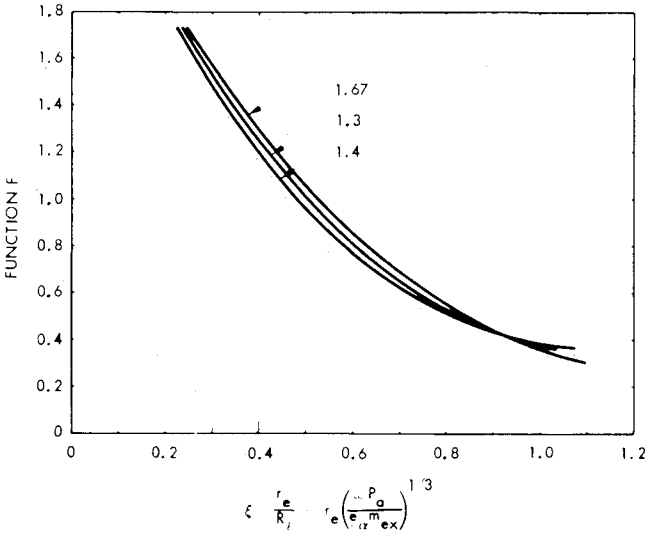

Fig. 5 Variation of the function F with r_e/R_ℓ.

Table 2 Variation of f_1, f_2, α, and G as a function of γ

γ	α	G	f_1	f_2
1.3	1.15	0.23	0.093	9.40
1.4	0.85	0.22	0.099	8.50
1.67	0.48	0.21	0.114	6.82

Table 3 Variation of the function ζ with conical half-angle θ

θ, deg	0	10	15	20
ζ	1.0	1.008	1.018	1.031

Table 4 Variation of the function η with conical half-angle θ

θ, deg	0	10	15	20
η	1.414	1.420	1.426	1.436

triatomic gas $\gamma = 9/7 = 1.29 \cong 1.3$, such as carbon dioxide; diatomic gas, $\gamma = 7.5 = 1.4$, such as nitrogen; and a monatomic gas, $\gamma = 5/3 \cong 1.67$, such as helium.

Values of the Jupiter mixture of 87.5% hydrogen and 12.5% helium, $\gamma = 1.43$, were obtained by interpolation.

The ratio of the radial length of the nozzle r_e to the characteristic length R_ℓ, i.e., r_e/R_ℓ, is an important parameter which relates the nozzle length to the characteristic blast wave length. The expression for R_ℓ is given by

$$R_\ell = [e_\alpha m_{ex}/(\omega P_a)]^{1/3} \tag{6}$$

where ω is the solid angle $2\pi(1-\cos\theta)$. As the ambient pressure, P_a, increases, the characteristic length, R_ℓ decreases; for a nozzle of given radial length, r_e, the ratio r_e/R_ℓ increases. When the blast wave reaches the characteristic length, R_ℓ, the predicted shock Mach number has decayed to a value of about 2; at a distance about 20% greater, the plateau pressure, P_0, behind the shock wave drops below the ambient pressure, P_a, signifying the onset of the rarefaction phase. By expressing the radial length of the nozzle in terms of the conical volume, the ratio r_e/R_ℓ is given by

$$r_e/R_\ell = \zeta[3VP_a/(e_\alpha m_{ex})]^{1/3} \tag{7}$$

where the function ζ depends upon the conical half-angle θ

$$\zeta = [2(1-\cos\theta)/(\sin^2\theta\cos\theta)]^{1/3} \tag{8}$$

The function ζ is a very weak function of the conical half-angle θ as indicated in Table 3. For the 10 deg half-angle nozzles used in the majority of the experiments, ζ is essentially unity so that the nondimensional length r_e/R_ℓ denoted by ξ is

$$\xi = [3VP_a/(e_\alpha m_{ex})]^{1/3} \tag{9}$$

The integral $H(\tau_e, \gamma)$ is dependent upon the variation of the plateau pressure ratio, P_0/P_a, with time, and depends upon the nondimensional time, τ_e, when the shock wave reaches the nozzle exit. For values of τ_e less than about 0.05, the integral H is positive, while for larger values of τ_e, H becomes negative (see, for example, Ref. 2). The approximate prediction from blast wave theory can be used for values of the ratio r_e/R_ℓ to about unity without too much error, and the relationship between τ_e and r_e/R_ℓ can be obtained from the result for the strong shock limit

$$\tau_e = [\alpha\gamma/(4\pi)]^{1/2}(r_e/R_\ell)^{5/2} \tag{10}$$

The function η in Eq. (3) is a very weak function of the conical half-angle θ, as indicated in Table 4. In addition, the variation of the function f_1 with γ is not great (see Table 2). Consequently, the essential form of the approximate prediction from blast wave theory using $\eta = 1.414$ and $f_1 = 0.10$ is as follows:

$$I \simeq 0.46(2e_\alpha\sigma/g_c)^{1/2}F \tag{2a}$$

where the function $F(r_e/R_\ell, \gamma)$ is the last bracketed term in Eq. (2),

$$F = 1 + \frac{15}{32(\pi)^{1/2}} f_2 H\left(\frac{r_e}{R_\ell}\right)^{1/2} \tag{11}$$

and is shown in Fig. 5. The function F is weakly dependent on γ and decreases with increasing r_e/R_ℓ because of rarefaction effects. At a value of r_e/R_ℓ of about 0.5, F becomes less than unity.

The form of the approximate prediction from blast wave theory suggests that the specific impulse data be plotted vs the ratio of $r_e/R_\ell = \xi$, as shown in Fig. 6. To generalize this representation, the specific impulse was normalized by dividing by the group $[(2e_\alpha/g_c)^{1/2}(1+\sigma)^{1/2}]$ based on a sim-

plified analysis from first principles.[2] In that analysis the gas mass in the nozzle, the sum of the explosive gases and ambient gas, $m=m_a+m_{ex}$, was taken to be accelerated to an average velocity and exhausted from the nozzle at the ambient pressure. The energy released in the explosion was presumed to increase the total enthalpy of the mass of gas, m, and this thermal energy in turn was taken to be converted completely into kinetic energy at the nozzle outlet. Thus, an upper bound on the specific impulse can be estimated which is

$$I=\lambda(2e_\alpha/g_c)^{1/2}(1+\sigma)^{1/2} \tag{12}$$

where λ is the divergence factor

$$\lambda=(1/2)(1+\cos\theta) \tag{13}$$

Since for the 10 deg half-angle nozzles used in the majority of the experiments, λ is essentially unity, the limiting value of the group

$$I/[(2e_\alpha/g_c)^{1/2}(1+\sigma)^{1/2}]=\iota \tag{14}$$

is essentially unity.

The results that are shown in Fig. 6a are for all the ambient gases, types of nozzles, and test conditions that are separately shown in Figs. 6b-e for the various ambient gases. The results indicate that for small values of the nondimensional length, ξ,

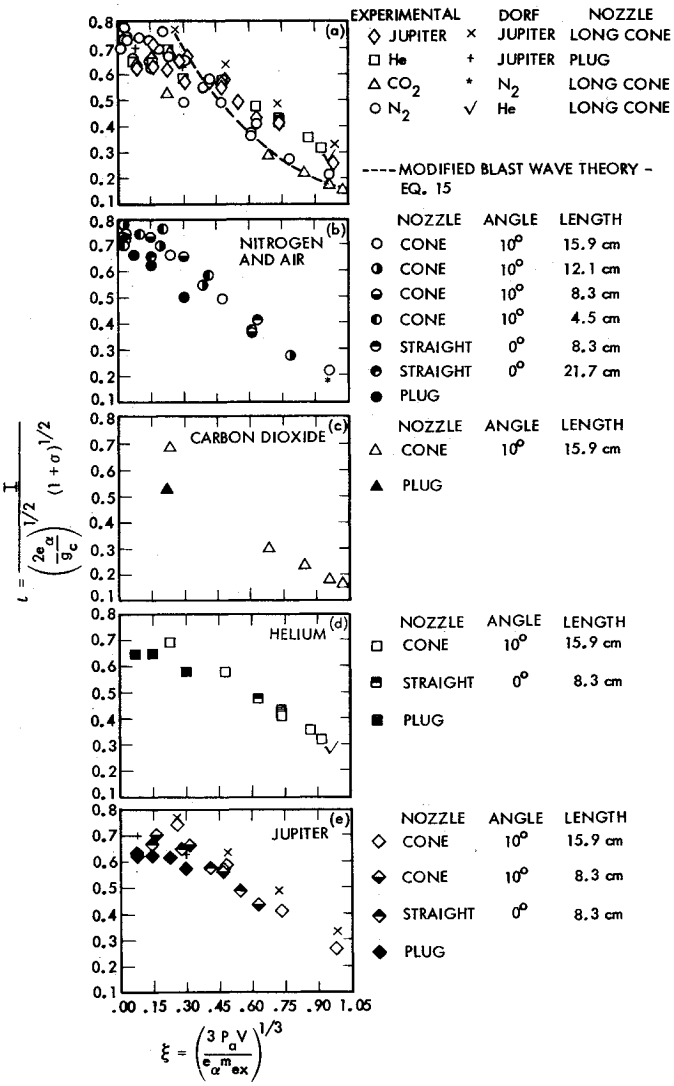

Fig. 6 Normalized specific impulse variation with nondimensional length, ξ, for all the ambient gases, types of nozzles, test conditions, and DORF calculations.

the normalized specific impulse is about 0.7 of the value calculated by the blast wave approximation, and with increasing values of ξ, decreases to a value of about 0.25 for ξ equal to unity. Although this representation does not precisely correlate the data with respect to the type of nozzle or the kind of ambient gas, it nevertheless does group all of the data reasonably well. Since the normalized specific impulses decrease with increasing ξ in a somewhat similar way as the function F shown in Fig. 5, the form of Eq. (11) suggests that an approximate correction to blast wave theory taking into account the explosive product gas might be to replace σ in Eq. (2) by $\sigma+1$, that is,

$$I\simeq 0.46(2e_\alpha/g_c)^{1/2}(1+\sigma)^{1/2}F \tag{15}$$

This modified prediction with average values for the function F obtained from Fig. 5 is shown by the dashed curve in Fig. 6a to be in reasonable agreement with the trend and approximate magnitude of the data for values of ξ between about 0.3 to 1.0. For small values of ξ, the modified prediction from blast wave theory would overestimate the data.

In the adaptation of blast wave theory to detonation propulsion, the exhaust plume was presumed to be conical and interaction with the surrounding envelope of ambient gas was not accounted for. In this ideal case the the nozzle is refilled by gas within the solid angle, ω, and a negative contribution to the impulse is calculated for the rarefaction and refilling phases. In this simplied view, the actual configurations of the charge and end wall were not accounted for, and the detailed nature of the kinetics of the explosion and the formation of the shock wave along with other wave motions were not considered. Frictional effects along the wall and heat transfer to the wall were also neglected, and the ambient gas contained in the nozzle was taken to be perfect gas with a constant value of γ so that existing solutions from blast wave theory could be utilized. Also, simplifications were made in evaluating the axial thrust and thus impulse integrals including counterpressure[3] over the duration of the expulsion, rarefaction, and refilling phases. Clearly, with these numerous simplifications, one would not expect to accurately calculate the specific impulse, although the prediction of the observed trends and approximate magnitude of the data over a range of values of ξ are noteworthy.

More recently, a numerical, time-dependent, two-dimensional, axisymmetric, inviscid calculation method (referred to as DORF) has been described that allows for a more appropriate treatment of the exhaust plume, refilling of the nozzle and oscillatory compression and rarefaction wave motion.[6,13] In this calculation method the explosive was assumed to be a thin disk completely covering the nozzle end wall, the detonation was assumed to be instantaneous ("volume burn" approximation), and the explosion product gas was assumed to follow the JWL equation of state.[5] The perfect gas law was used for the ambient gas, and any dissociation or ionization effects of shock heating were not considered. Also, frictional effects along the nozzle wall and heat transfer to the nozzle wall were neglected.

Two-dimensional numerical flow predictions (DORF) were primarily made on a CDC-7600 computer for the simulated Jupiter atmosphere for the long-cone and firing-plug nozzles and are shown in Fig. 7, where the data obtained with the various nozzles are shown. The specific impulse predictions are in agreement with the data trends described previously and lie above the data by 3-28%. Two other DORF predictions that were made are shown in Fig. 4 for the lone-cone nozzle with nitrogen and helium ambient gases at a pressure of 69 bars. In these cases, the predictions lie below the data by 10-15%. All of the DORF predictions are also shown in the representation of Fig. 6 and indicate the trend and approximate magnitude of the normalized specific impulse data with increasing nondimensional length ξ.

Rarefaction and Oscillatory Wave Phenomena

The pressure-time history at two locations on the long-cone nozzle wall was measured by two Kistler 603 HI piezoelectric crystal pressure transducers which were placed flush on the inside of the conical wall at 10.8 and 14.6 cm axially from the end wall. The rise time of the transducers and the filters (maximum cutoff frequency = 330 kHz) in the charge amplifiers (Kistler 5002 Y057) was 1 μs. Nozzle vibration or ringing transmitted to the transducers was effectively removed by mounting the transducers in a mixture of silicon grease and soft polyurethane foam that provided enough viscous resistance along with the inertia of the transducer to withstand pressures on the order of hundreds of bars and remain in place during the short duration times. The pressure signal was believed to be of good quality and to indicate accurately the transient behavior reported herein.

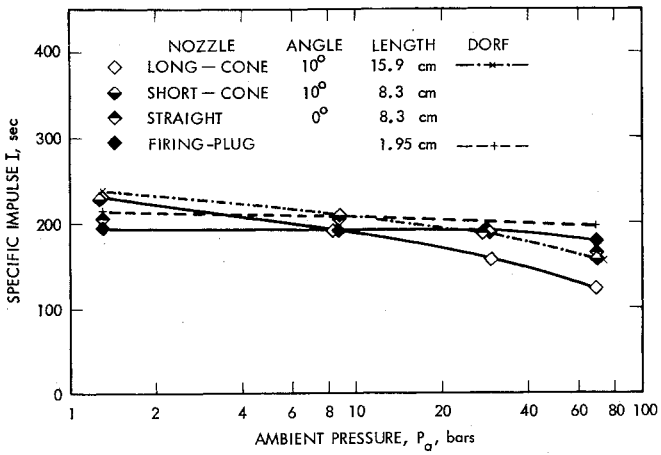

Fig. 7 Specific impulse for the simulated Jupiter atmosphere with various types of nozzles.

The pressure-time histories at the two pressure transducer locations A and B are shown in Figs. 8 and 9 for helium and nitrogen, respectively, at an ambient pressure of 69 bars. The time scale in the upper half of these figures is 50 μs/division, while in the lower half it is 10 times greater, 500 μs/division, in order to reveal the longer transient behavior. From the abrupt rise in pressure accompanying the arrival of the blast wave generated by the detonation, the calculated average speed of the shock front between the two transducer locations was 2.3 and 0.77 km/s in helium and nitrogen, respectively. These speeds correspond to shock Mach numbers of 2.25 and 2.19, respectively. Since the sound speed is a factor of 2.89 higher in helium than nitrogen, shock speeds are also expected to be higher at the same ambient pressure in helium than nitrogen; the shock speed ratio was nearly the same as the sound speed ratio. Assuming as time origin the rupturing of a wire buried in the explosive, the time of arrival of the shock front at transducer location A was 35 and 78 μs in helium and nitrogen, respectively. Further details on the blast wave in the nozzle which exhausts the ambient gas and some of the products of detonation after passing outside the nozzle are given in Ref. 5.

The pressure relaxed after arrival of the blast wave, eventually becoming less than the ambient value. The initial part of this rarefaction phase has been previously observed by Filler.[14] The present measurements of longer duration revealed a significant amount of rarefaction; the minimum pressures became as low as about 0.1 and 0.4 of the ambient pressure in helium and nitrogen, respectively. The pressure rises subsequently during the beginning of the partial refilling phase. In particular, in helium (Fig. 8a) the pressure rises

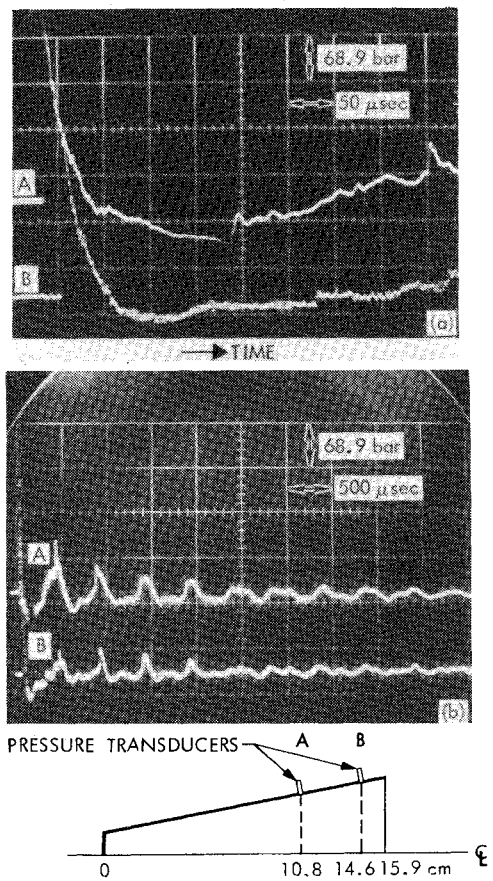

Fig. 8 Pressure vs time profiles at two transducer locations; ambient gas helium; ambient pressure = 68.9 bars: a) time = 50 μs/division; b) time = 500 μs/division.

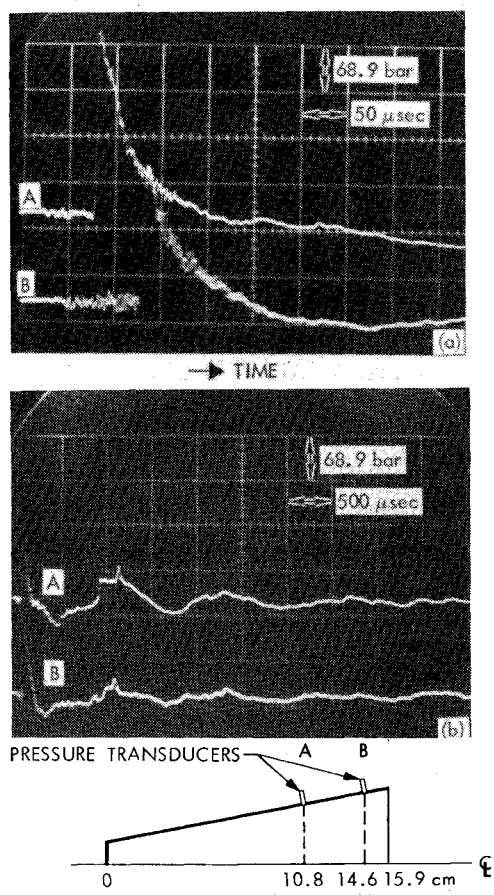

Fig. 9 Pressure vs time profiles at two transducer locations; ambient gas nitrogen, ambient pressure = 68.9 bars: a) time = 50 μs/division; b) time = 500 μs/division.

more gradully at transducer location B nearer the nozzle exit, while, at a short time later, there is a more abrupt rise in pressure at transducer location A further in the nozzle. This pressure sequence is believed to be associated with the steepening of compression waves propagating into the rarefaction region near the nozzle exit, thus forming a shock wave that propagated back toward the end wall. The pressure continued to increase gradually as a result of more incoming compression waves from the outside, until the reflected shock from the end wall passed the transducer location, as indicated by the spike in the signal shown in Figs. 8 and 9. The pressure then decreased to below the ambient pressure again as some gas flowed out of the nozzle in the second expansion phase. The next cycle then began because of rarefaction in the nozzle, again inducing compression wave motion and partial refilling.

The oscillatory wave and flow behavior for helium had a period of about 500 μs. The average wave speed for the four traverses of the nozzle length for the compression and expansion phases was 1.3 km/s, a value that was about 30% higher than the speed of sound in ambient helium. In nitrogen the period was longer than for helium by a factor of about 2.5, which again was about the same magnitude as the sound speed factor mentioned previously. The subsequent pressure oscillations decayed in amplitude owing to the weakening of the strength of the waves with time and viscosity. Over the short time of the measured signal, the period of oscillations remained about the same. The wave phenomenon was similar in principle although more complex in nature than that for a compressed gas in a tube suddenly opened to the atmosphere at one end.[15]

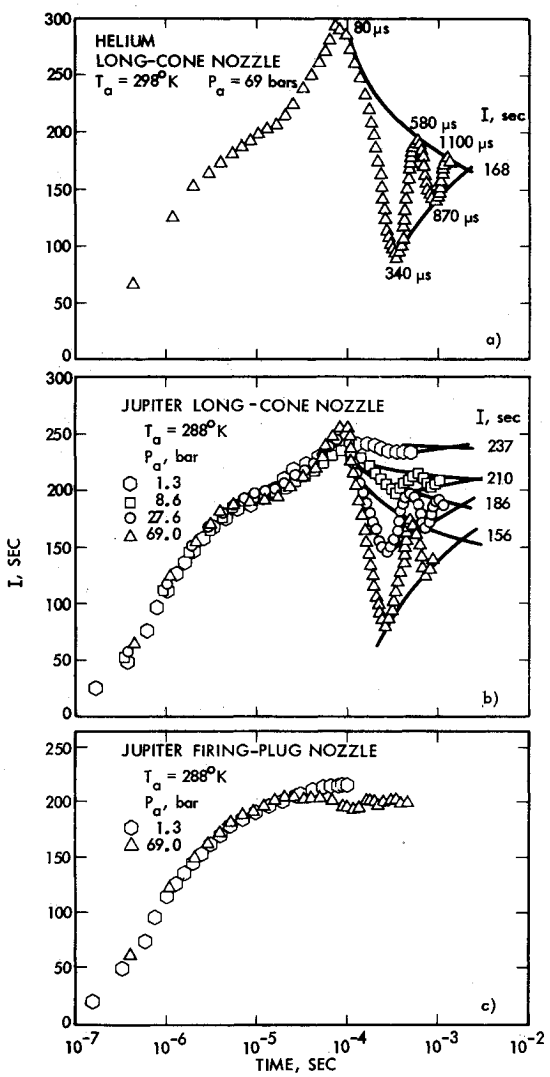

Fig. 10 Predicted transient and asymptotic specific impulses using DORF model: a) helium, long-cone nozzle; b) Jupite, long-cone nozzle; c) Jupiter, firing-plug nozzle.

The time-dependent, two-dimensional, inviscid flow calculations (DORF) provide a more detailed view of the influence of the rarefaction and oscillatory wave phenomenon on the specific impulse as indicated by the time varying behavior

$$I(t) = \frac{1}{m_{ex} g_c} \int_0^t \int_A (P - P_a)\, dA\, dt \tag{16}$$

where $P - P_a$ is the pressure difference acting on the nozzle wall, A is the nozzle cross-sectional area, and t is time. Clearly, when the integrated pressures along the inside of the nozzle wall drop below the ambient pressure, there is a negative contribution to the specific impulse. The predicted variation of specific impulse with time is shown for the long-cone nozzle with helium at an ambient pressure of 69 bars in Fig. 10a. Results can be directly compared to the measured pressure-time history at the particular locations shown in Fig. 8. The specific impulse increased to a peak value of about 300 s at about 80 μs, and then decreased in magnitude as the pressure became less than ambient to a minimum value of about 80 s at 340 μs, at which time the pressure became greater than ambient again, and the specific impulse increased again. Subsequent local peaks and minimums that decreased in magnitude occurred at the times indicated, which correspond to pressures becoming less than or greater than ambient pressure, respectively. The oscillatory variation of the specific impulse was estimated to eventually reach an asymptotic value of 168 s, a value about 10% below the extrapolated measured value. The predicted period of 500-530 μs in the specific impulse oscillations was in good agreement with the period of about 500 μs in the measured pressure oscillations. Of particular note is the significant decrease in the final impulse from the peak value because of rarefactions. Similar results were noted for the long-cone nozzle with nitrogen at an ambient pressure of 69 bars.[6]

With some confidence in the DORF predictions established, attention is now focused on the trends of the simulated Jupiter atmosphere data shown in Fig. 7, where it is evident that the specific impulse is greater for the plug nozzle at higher ambient pressures, but greater for the long-cone nozzle at low ambient pressures. The prediction of the variation of the specific impulse with time is shown in Fig. 10b for the long-cone nozzle and in Fig. 10c for the plug nozzle. For the long-cone nozzle (Fig. 10b), the specific impulse is essentially independent of the ambient pressure for times up to about 50 μs, with the peak value about 240 s. At the highest ambient pressure, the oscillatory variation in the specific impulse associated with rarefactions is largest, and the asymptotic value is considerably reduced below the peak value in a similar way, as was noted for helium. The oscillatory period for the simulated Jupiter atmosphere was about 380 μs, a factor of about 0.75 that for helium, which corresponds to the higher sound speed of a ratio of 4/3 in the simulated Jupiter atmosphere compared to helium. As the ambient pressure decreased, the magnitude of the specific impulse oscillations diminished, and the asymptotic value became closer to the peak value. At the lowest ambient pressure, rarefaction effects were essentially negligible and the highest specific impulse was predicted.

With the firing-plug nozzle (Fig. 10c), the variation in specific impulse with time was different than for the long-cone nozzle. At the highest ambient pressure, 69 bars, rarefaction effects hardly changed the specific impulse from the peak value of about 200 s, and, therefore, the asymptotic value was considerably greater than that for the long-cone nozzle. On the other hand, at the lowest ambient pressure where rarefaction effects were essentially negligible in either type of nozzle, the specific impulse was greater in the long-cone nozzle. The predicted decrease in specific impulse with

increasing pressure for the plug nozzle was about 10%, similar to the measurements.

Design Considerations for a Flight System

From the data and the analyses it is apparent that the design of an optimum nozzle for a flight system is dependent on the ambient gas if the maximum specific impulse and minimum system mass are to be obtained. Detonation within a nozzle with a small angle of divergence directs the gas flow and, therefore the specific impulse or thrust from a single detonation is increased over a larger half-angle nozzle[2] or a flat plate. When the nozzle is filled with a gas of high density, the shock wave, in passing through this gas, accelerates the ambient gas, and the ambient gas is discharged from the nozzle at high velocity along with the explosive gas. This additional mass contributes to the thrust provided by the explosive and is reflected directly in specific impulse for the explosive and nozzle system. If the nozzle expansion ratio or length is too great, the blast wave from the detonation overexpands the gases in the nozzle and the pressure becomes less than the ambient pressure by significant amounts. This overexpansion causes oscillating gas flows within the nozzle, and when integrated with time, reduces the impulse delivered from a single detonation. An optimum design nozzle for maximum impulse in this case should be either short (note that any addition in nozzle length also adds mass to the vehicle system), or the nozzle should have some kind of device that can modify refilling of the nozzle with amibient gases to prevent overexpansion, oscillations, or unbalanced forward pressure forces.

Our data currently indicate that the lower molecular weight gases, in which sonic speeds are higher, result in 1) less mass of gas in the nozzle and 2) shorter nozzle axial lengths before ambient gas overexpansion becomes important. The optimum nozzle length for low molecular weight gases thus tends to be short.

Detonation propulsion technology can be considered for use with large velocity changes as a main propulsion system or with small velocity changes such as attitude control propulsion. These designs must consider both the rapidity of the detonation pulses and the vehicle velocity relative to the exhaust gas. For attitude control systems with low pulse rates, the optimum design would be short nozzles for low molecular weight ambient gases. For applications where the pulse rate is very rapid (i.e., milliseconds between pulses) or low relative vehicle velocity (less mixing), the ambient gas that fills the nozzle is not only the atmospheric ambient gas, but a combination of the explosive products and the atmospheric ambient gas. Under this rapid fire condition it would not be necessary to minimize the length of the nozzle because of low molecular weight ambient gas effects. The molecular weight of the explosion products of typical explosives is the weighted average of carbon monoxide, carbon dioxide, water, hydrogen, and some nitrogen. If the explosive has a high oxygen content, then it will have a high molecular weight. With an explosive gas with mean molecular weight of 25 to 30, the performance would be like that of nitrogen, and a longer length would be optimum. With underoxidized explosives the molecular weight would be lower (Deta sheet "C" is estimated to about 18) and shorter nozzles may be optimum. The explosive product and ambient gas temperatures also affect the density of the gases in the nozzle and, therefore the mass of gas contained in the nozzle after rapid firings, but little is known about performance under these conditions either experimentally or from predictions. In the DORF code written for the current single-firing investigation, the initial gas contained in the nozzle is the atmospheric ambient gas, not a combination of the explosive product gas remaining from a preceding firing and the atmospheric ambient gas.

From our data the following design criteria are determined for nozzles like those tested.

1) For a slow pulse rate—the nozzle filled with ambient atmospheric gas—the nozzle should be short if the molecular weight of the ambient gas is low, and long if the ambient gas has a high molecular weight.

2) For a rapid rate of firing, the nozzle should be designed for the ambient gas with due consideration being given to the explosive gas products.

3) If the flight velocity is low—for which the explosive product gases are mixed rapidly with the ambient gas—then consideration should be given to shorter nozzles because of the expected dilution of the explosive product gas by the ambient gas.

4) If the gas density is low owing to higher temperatures or lower pressures so that σ is low, the nozzle should be short.

Acknowledgments

The research described in this paper was performed by the Jet Propulsion Laboratory, California Institute of Technology, under contract with the National Aeronautics and Space Administration. The authors express their gratitude to Mr. Winston Gin, who conceived this concept for propulsion in dense planetary atmospheres, Dr. R. F. Cuffel, who carried out the two-dimensional numerical flow calculations (DORF) on a CDC-7600 computer, Dr. K. Kim for the data he obtained from nozzle wall pressure measurements, and Ms. C. R. Glazer for data reduction and the calculations from blast wave theory. The technical efforts of Mr. Ralph Morrow and Mr. Anthony H. Ramussen during the experimental phase are also greatly appreciated.

References

[1] Varsi, G., Back, L. H, and Dowler, W. L., "Development of Propulsion for High-Atmospheric-Pressure or Dense Environments," Jet Propulsion Lab., *Quarterly Technical Review*, Vol. 3, No. 2, 1973.

[2] Back, L. H. and Varsi, G., "Detonation Propulsion for High Pressure Environments," *AIAA Journal*, Vol. 12, Aug. 1974, pp. 1123-1130.

[3] Back, L. H., "Application of Blast Wave Theory to Explosive Propulsion," *Acta Astronautica*, Vol. 2, No. 5/6, 1975, pp. 391-407.

[4] Kim, K., Back, L. H., and Varsi, G., "Measurements and Calculations of Detonation Propulsion Performance in Helium," *AIAA Journal*, Vol. 14, March 1976, pp. 310-312.

[5] Varsi, G., Back, L. H., and Kim, K., "Blast Wave in a Nozzle for Propulsion Applications," *Acta Astronautica*, Vol. 3, 1976, pp. 141-156.

[6] Kim, K., Varsi, G., and Back, L. H., "Blast Wave Analysis for Detonation Propulsion," *AIAA Journal*, Vol. 15, Oct. 1977, pp. 1500-1502.

[7] Yang, L. C., "Performance Characteristics and Statistics of a Laser Initiated Microdetonator," *Proceedings of the 10th Symposium on Explosives and Pyrotechnics*, Franklin Institute, Philadelphia, Feb. 1979.

[8] *The Planet Jupiter*, NASA SP-8069, Dec. 1971.

[9] *The Planet Saturn*, NASA SP-9091, June 1972.

[10] Sedov, L. I., *Similarity and Dimensional Methods in Mechanics*, Academic Press, New York, 1959, p. 210.

[11] Korobeinikov, V. P., Chushkin, P. I., and Sharovatova, K. V., *Tables of Accurate Gas Dynamic Functions of the Initial Phase of Explosions*, Issue 2, Computing Center of Academy of Sciences, USSR, Moscow (in Russian), 1963.

[12] Korobeinikov, V. P., Chushkin, P. I., and Sharovatova, K. V., *Accurate Gas Dynamic Function for Explosions*, V. P. Karlikov, ed., Computing Center of Academy of Sciences, USSR, Moscow (in Russian), 1969.

[13] Kim, K. and Johnson, W., "Exit of a Blast Wave from a Conical Nozzle," AIAA Paper 76-401, San Diego, Calif., July 1976.

[14] Filler, W. S., "Measurements on the Blast Wave in a Conical Tube," *Physics of Fluids*, Vol. 3, No. 3, 1960, pp. 444-448.

[15] Rudinger, G., *Wave Diagrams for Nonsteady Flow in Ducts*, D. Van Nostrand Co., Inc., 1955, p. 186.